Renewable and Responsive Cross-Linked Systems Based on Polyurethane Backbones from Clickable Biobased Bismaleimide Architecture

Khantutta-Kim Tremblay-Parrado, Clément Bordin, Samuel Nicholls, Benoit Heinrich, Bertrand Donnio, Luc Avérous

Renewable and Responsive Cross-Linked Systems Based on Polyurethane Backbones from Clickable Biobased Bismaleimide Architecture

Khantutta-Kim Tremblay-Parrado, Clément Bordin, Samuel Nicholls, Benoit Heinrich, Bertrand Donnio, Luc Avérous*

Cite this: *Macromolecules* 2020, 53, 5869–5880
Publication Date:July 17, 2020
https://doi-org.scd-rproxy.u-strasbg.fr/10.1021/acs.macromol.0c01115

Abstract

A new biobased bismaleimide architecture from methyl oleate, consisting of an aliphatic branched structure, denoted methyl oleate bismaleimide (MO BMI), was synthesized and fully characterized. MO BMI was used as a cross-linking agent to obtain networks by using linear biobased furan bearing PUs via the Diels–Alder reaction and compared with more conventional aromatic or aliphatic bismaleimides (BMIs). These networks can be defined as dissociative covalent adaptable networks (CANs). Different linear biobased PUs were synthesized by using rapeseed-based polyol, hexamethylene diisocyanate, and (furan-2,5-diyl)dimethanol as a chain extender. The furan content was controlled by varying the hard segment content. Compared to conventional BMIs, MO BMI as biobased cross-linker impacts particularly the materials performance and the mechanical properties, for example an increase of the elasticity. MO BMI also yields most consistent advanced properties in terms of thermal recyclability and self-healing.

Introduction

Polymer science has been established as a distinct field of organic chemistry for over 100 years.[1,2] Since that era, the invention of plastics has drastically changed our daily lives. However, most plastics are based on synthetic macromolecules that originate from nonrenewable petroleum resources.[3] Recently, the worldwide polymer industry has performed considerable progress to ensure the development of sustainable polymers with lower environmental impact using renewable feedstocks. Nevertheless, continued progress for these materials to contain advanced materials properties such as a controlled end-of-life to improved waste management is still required.

Renewable feedstocks are very diverse such as vegetable oils, woods, sugars, and polysaccharides from annual cultures. Plant oils are of particular interest as their innate chemical architectures allow for a vast panel of potential chemical modifications.[4] They are also of interest from an industrial

perspective, as they are highly accessible at rather low production cost with low toxicity.[5] Vegetable oils as well as their fatty acid derivatives have been widely used for the synthesis of polymers such as polyesters,[6,7] polyamides,[8,9] epoxy resins,[10] and quite prominently polyurethanes (PUs).[11−14]

PUs are a leading polymer family, with their production ranked sixth among all polymers.[15] Because of their wide structural variability, PUs are used for applications such as, the building, transportation, and furniture industries.[16] Although the use of plant oils for the synthesis biobased PUs is on the raise,[17] limited research has exploited these biobased structures to develop advanced materials, to achieve for instance, dynamic and adaptable materials with high recyclability and extended lifetimes.

In the past 20 years, the introduction of dynamic cross-links in polymers has developed a new generation of polymer materials that can be reprocessed like thermoplastics, all the while maintaining the benefits of thermosets. This incorporated feature allows for the possibility of advanced properties such as healing, reprocessability, and extended material lifetimes and can reduce the consumption of energy and resources as well as reduce waste.[18] These networks have been defined as covalent adaptable networks (CANs)[19] based on dynamic covalent bonds that can assemble and disassemble by “dissociative” or “associative” means when exposed to specific stimuli.[20] In associative CANs, dynamicity occurs by a substitution reaction between an existing cross-link and a pending reactive group, whereas in dissociative CANs, cross-links are cleaved back into their individual reactive moieties before re-forming again. Dissociative CANs have been predominately studied[21−23]—more specifically those cross-linked via Diels–Alder (DA) adducts formed between furan and maleimide moieties. The DA reaction between furan and maleimide functions is defined as a click cycloaddition reaction and occurs at modest temperatures (below 90 °C), whereas the retro-DA (r-DA) reaction occurs predominately between 110 and 130 °C.[24] Although there have been increasing reports of biobased CANs, associative[25] and dissociative[21,26−30] alike, limited research has explored the use of the thermoreversible DA in biobased cross-linked PUs.[31−33]

The aim of this study is to explore reversible cross-linked PUs based on vegetable oils using the thermally reversible furan–maleimide DA reaction, with a particular interest in studying the changeability of cross-links localized on hard segments and the use of an original and biobased bismaleimide. As depicted in Scheme 1, (furan-2,5-diyl)dimethanol (FDM) is used as a furan bearing chain extender incorporated into the linear polymer backbone and further cross-linked with the use of different bismaleimides (BMIs). In this frame, we report the synthesis of a new methyl oleate-based BMI (MO BMI), which to our knowledge is the first of its kind. The topic of the synthesis and use of maleimide-bearing architectures having recently been explored in depth by Dolci and co-workers affirms this, as no such architectures were reported.[34] The use of this new MO BMI is compared to aromatic and aliphatic fossil-based BMIs. These fossil-based BMIs are commercially available. The aromatic bismaleimide chosen was 1,1′-(methylene di-4,1-phenylene)bismaleimide (MP BMI), and the aliphatic fossil-based bismaleimide chosen was a polypropylene (PPO)-based BMI (PPO BMI) with a degree of polymerization (DP) of 3. The corresponding materials were synthesized with varying furan contents and different cross-linkers. They are studied for advanced properties such as thermal reprocessability and self-healing ability.

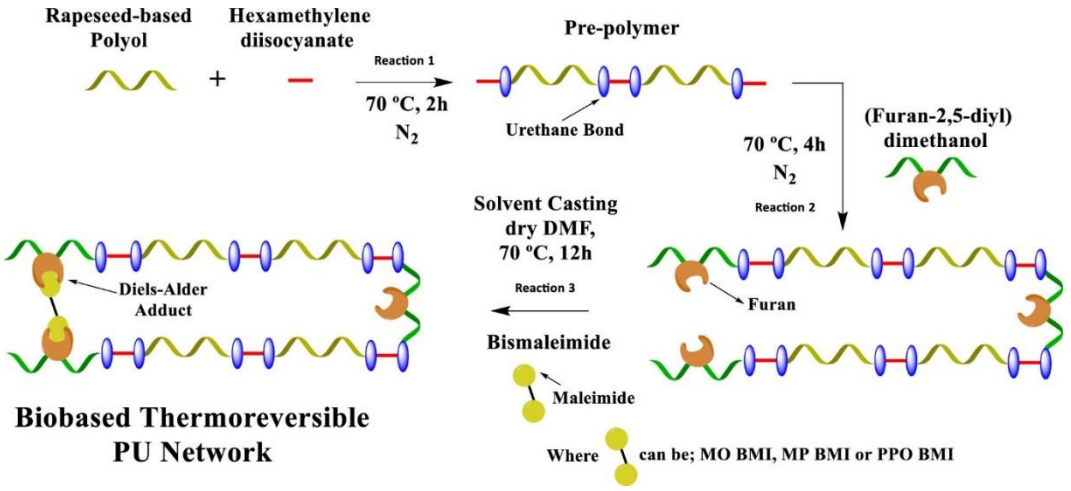

Scheme 1. Illustration of the General Synthesis of Biobased Thermoreversible PU-Based Systems Using (Furan-2,5-diyl)dimethanol and Different BMIs (MO BMI, MP BMI, and PPO BMI)

Experimental Section

Reagents and Materials Methyl oleate (MO) from sunflower oil was kindly supplied by ITERG (France). It is a fatty acid with an acid value of 0.34 mg KOH/g and an iodine value of 77 g of I_2/100 g. Biobased polyester polyol (purchased from Oleon, France) was derived from dimeric fatty acids from rapeseed oil with purity greater than 98% and weight-average molar mass (M_w) around 3000 g/mol. Hydroxyl and acid values were 33.7 and 0.253 mg/g of KOH, respectively. 2-Chloro-4,4,5,5-tetramethyl-1,3,2-dioxaphospholane (CL-TDP, 95%), 6-maleimidohexanoic acid (6-MHA, 95%), hydrogen peroxide (H_2O_2, 30% w/v aqueous solution), chromium(III) acetylacetonate (99.99%), [D_6]dimethyl sulfoxide (DMSO, 100%, 99.96% atom D), chloroform-*d* ($CDCl_3$, 100%, 99.96% atom D), amberlyst 15, 1,4-butanediol (BDO, 98%), oxalyl chloride (99%), and cholesterol (>99%) were purchased from Sigma-Aldrich. 1,1′-(Methylene di-4,1-phenylene)bismaleimide (95%, MP BMI) was purchased from Alfa Aesar. *N*,*N*-Dimethylformamide (DMF, 99.8%), chloroform (99.8% stabilized with amylene), glacial acetic acid (GAA, >99%), and ethyl acetate (EA, 95%) were purchased from Fisher Scientific. Amberlite IR-120 H was from Fluka Chemicals. Poly(propylene oxide)-based bismaleimide (PPO BMI) with DP_n = 3 was obtained from Specific Polymers (Castries, France). 2,3,4,5,6-Pentafluorobenzaldehyde (PFB, 98%) and (furan-2,5-diyl)dimethanol (FDM, 97%) was purchased from Fluorochem. Reagents and solvents from commercial suppliers were used without additional purification.

Syntheses and Materials Preparations *Epoxidation of Methyl Oleate from Sunflower Oil* The epoxidation of methyl oleate (MO) was conducted by the in situ formation of peracetic acid from glacial acetic acid and H_2O_2 and was adapted from Arbenz et al.[35] In a two-necked round-bottom flask, equipped with a magnetic stirrer and a dropping funnel, MO (1 mol equiv of unsaturations), Amberlite IR-120 H (25 wt % of MO), and glacial acetic acid (0.5 mol equiv) were inserted into the flask and dissolved at 0.5 mL/g of MO in toluene. The solution was stirred to 70 °C, and then 1.5 mol equiv of H_2O_2 was added dropwise. The mixture was stirred at 70 °C for 7 h. The solution was diluted in ethyl acetate. The Amberlite IR-120 H was filtered off, and the solution was washed with distilled water until a neutral pH was attained. The organic phase was dried with anhydrous sodium sulfate and then filtered. The solvent was evaporated under reduced pressure. Methyl 8-(3-octyloxiran-2-yl)octanoate (MOO) was dried under vacuum overnight at 50 °C. The reaction product, methyl 8-(3-octyloxiran-2-yl)octanoate (MOO), was a clear light yellow oil.

Methyl 8-(3-Octyloxiran-2-yl)octanoate (MOO) ^{1}H NMR (400 MHz, $CDCl_3$): δ = 3.63 (s, 3H, (C═O)OC*H*$_3$), 2.9 (m, 2H, C*H*OC*H*), 2.3 (t, 2H, C*H*$_2$C(═O)), 1.6 (m, 2H, C*H*$_2$CH$_2$C(═O)), 1.3–1.0 (m, 24H, aliphatic CH_2), 0.9 (t, 3H, C*H*$_3$). ^{13}C NMR (400 MHz, $CDCl_3$): δ: 174 (*C*═O), 57.2 (O*C*H$_3$), 57.2 (H*C*–O–*C*H), 51.4 (O*C*H$_3$), 34.0 (*C*H$_2$–C(═O)), 31.9–22.7 (aliphatic *C*H$_2$), 14.1 (*C*H$_3$).

Ring-Opening by Butane-1,4-diol of Methyl 8-(3-Octyloxiran-2-yl)octanoate In a round-bottom flask, equipped with a magnetic stirrer, MOO (1 mol equiv of epoxy), Amberlyst 15 (4 wt % of MOO), and butane-1,4-diol (10 mol equiv) were introduced. The mixture was stirred at 75 °C for 10 h. The solution was diluted in ethyl acetate, and the Amberlyst 15 was filtered off. The solution was washed with distilled water until a neutral pH was attained, and the excess of BDO was removed. The organic phase was dried with anhydrous sodium sulfate and then filtered. The solvent was evaporated under reduced pressure. Methyl 10-hydroxy-9-(4-hydroxybutoxy)octadecanoate (MO Diol) was dried under vacuum overnight at 50 °C. The reaction product, MO Diol, was a clear light yellow oil.

Methyl 10-Hydroxy-9-(4-hydroxybutoxy)octadecanoate (MO Diol) ^{1}H NMR (400 MHz, $CDCl_3$) δ: 3.63 (s, 3H, (C═O)OC*H*$_3$), 3.65–3.45 (m, 1H, C*H*OH) and (m, 2H, C*H*$_2$OH), 3.47 (t, 2H, C*H*$_2$OCH), 3.10 (q, 1H, CH$_2$OC*H*), 2.3 (t, 2H, C*H*$_2$C(═O)), 1.6 (m, 2H, C*H*$_2$CH$_2$C(═O)), 1.3–1.0 (m, 28H, aliphatic C*H*$_2$), 0.9 (t, 3H, C*H*$_3$). ^{13}C NMR (400 MHz, $CDCl_3$) δ: 174 (C═O), 83.0 (CH$_2$*C*HOH), 72.7 (*C*HOH), 70.5 (*C*H$_2$CHOH), 51.4 (O*C*H$_3$), 34.0 (*C*H$_2$–C(═O)), 31.9–22.7 (aliphatic CH_2), 14.1 (*C*H$_3$).

Chlorination of 6-Maleimidohexanoic Acid 6-MHA (1 mol equiv) was placed in a two-necked, flame-dried round-bottomed flask flushed with argon and charged with a magnetic stirring bar. Anhydrous ethyl acetate was then added, and the solution was cooled to 0 °C under a flow of nitrogen. An excess of oxalyl chloride (1.5 mol equiv) was then added dropwise at 0 °C (15 min) and finally heated at 50 °C for 3 h. The excess of oxalyl chloride and solvent was evaporated under vacuum. The product, 6-maleimidoundecanoyl chloride (6-MHC), was obtained as a low-melting yellow solid and used without any further purification.

6-Maleimidohexanoyl Chloride (6-MHC) ^{1}H NMR (400 MHz, $CDCl_3$, δ (ppm)): 6.69 (s, 2H, C*H*–ring), 3.56 (t, 2H, C*H*$_2$–N), 2.89 (t, 2H, C*H*$_2$(C═O)Cl), 1.71 (m, 2H, C*H*$_2$CH$_2$(C═O)Cl), 1.60 (m, 2H, C*H*$_2$CH$_2$–N), 1.3 ppm (m, 2H, C*H*$_2$CH$_2$CH$_2$–N). ^{13}C NMR (400 MHz, $CDCl_3$) δ: 174 ((*C*═O)Cl), 170 (*C*O–ring), 135 (*C*H–ring), 46.7 (CH$_2$(C═O)Cl), 39.0 (*C*H$_2$N), 29.3–25.0 (aliphatic chain carbons).

Synthesis of Methyl Oleate Bismaleimide (MO BMI) MO Diol was esterified with 1.2 equiv of 6-MHC with respect to the amount of total hydroxy groups. In agreement with different green chemistry principles, the reaction was catalyst-free at 65 °C. $CHCl_3$ was added to homogenize the reaction mixture. At the end of the reaction, a brown viscous product was obtained. Methanol was added to quench the unreacted 6-MHC, and the mixture was left stirring for an additional 30 min. The solvents were then evaporated under vacuum, and the resultant MO BMI products finally dried under high vacuum for 24 h

Methyl Oleate Bismaleimide (MO BMI) ^{1}H NMR ($CDCl_3$, 400 MHz) δ: 6.69 (s, 4H, C*H*–ring), 4.61 (m, 1H, C*H*O(C═O)), 4.06 (t, 2H, (C═O)OC*H*$_2$), 3.63 (s, 3H, (C═O)OC*H*$_3$), 3.56 (t, 4H, C*H*$_2$–N), 3.47 (t, 2H, C*H*$_2$OCH),), 3.25 (q, 1H, CH$_2$OC*H*), 2.30 (m, 6H, CH$_2$(C═O)O), 1.20–1.80 (multi, 40H, CH_2), 0.9 (t, 3H,CH$_3$). ^{13}C NMR (400 MHz, $CDCl_3$) δ: 174 (CH$_2$(*C*═O)), 171 (*C*O–ring), 134 (*C*H–ring), 51.4 (O*C*H$_3$), 39.0 (*C*H$_2$N), 34.0 (*C*H$_2$–C(═O)), 31.9–22.7 (aliphatic CH_2), 14.1 (*C*H$_3$).

Study of the DA Reaction between MO BMI and FDM MO BMI (200 mg) was dissolved in [D_6]DMSO (2 mL) in a 10 mL round-bottom flask. (Furan-2,5-diyl)dimethanol (FDM) was added to obtain a furan/maleimide ratio of 1:1 (mol/mol). The solution was placed in an oil bath regulated to 65 °C, and samples (200 µL) were taken at regular intervals over 4 days. The samples were further diluted to 650

μL and analyzed by ^{1}H NMR to determine the reaction conversion and *endo/exo* ratio of the DA adducts.

Synthesis of PUs Based on FDM All glassware and reactants were previously dried. PUs were synthesized by a two-step polymerization process. Three different kinds of PUs films were prepared by a two-step synthesis process by varying the content of hard segments (HS) in wt %, based on diisocyanate and FDM, by 5, 10, and 20%. First, for the prepolymerization step, in a three-necked round-bottom flask flushed with nitrogen, the biobased rapeseed polyester polyol was added to hexamethylene diisocyanate (HDI), and the mixture was mechanically stirred at 70 °C for ∼2 h until an appropriate NCO value was attained.

During the synthesis, aliquots were extracted to determine the NCO content to control and follow the NCO consumption during the reaction. A specific method has been performed to determine isocyanate content by reaction with 1 equiv of *N*-dibutylamine to give NCO content (in wt %). The prepolymer sample (≈1.2 g) was diluted in a standard solution (20 mL) of dibutylamine (0.2 M) in THF for the reaction with the unreacted diisocyanate. The amine excess was back-titrated with a 0.5 aqueous solution of HCl. The NCO content (wt %) was determined via eq 1:

$$\%\mathrm{NCO} = \frac{(V_{\mathrm{blank}} - V_s) \times 42 \times 0.1}{m_s} \quad (1)$$

in which V_{blank} (mL) is the HCl solution volume required for a blank titration of the dibutylamine solution, while V_s is the volume required for the prepolymer titration and m_s is the prepolymer weight. This result was used for the addition for the precise amount of FDM. The appropriate amount of FDM is dissolved in anhydrous DMF (1 mL/g FDM) and added to the above-mentioned reaction system and stirred for 3 h. The ratio of −NCO/–OH functional groups was fixed to 1.05 in all cases.

Cross-Linking of PUs by Each BMI The PU was dissolved in anhydrous DMF. The respective amount of each bismaleimide was added in a 1:1 furan to maleimide ratio (mol/mol). The reaction mixture was stirred at 70 °C for 12 h to allow for the DA adducts to form. The solution was poured into a polytetrafluoroethylene mold and put into the oven to evaporate the solvent (70 °C, 48 h). Solvent traces were removed under vacuum at 70 °C for 24 h. Cross-linked PU systems using MO BMI were labeled PU-HS5-MOBMI, PU-HS10-MOBMI, and PU-HS20-MOBMI. Two additional cross-linked PUs were obtained by using linear PU-HS20 with cross-linked with a reference and conventional BMI, MP BMI, or PPO BMI and denoted as PU-HS20-MPBMI or PU-HS20-PPOBMI.

Study of the Reprocessability Behavior of PUs PU films were reprocessed by compression molding in a tile mold (10 cm × 10 cm × 1 mm) at 140 °C in a LabTech Scientific press hot press. First, the films were cut in several small pieces and placed in the center of the tile and left to undergo a 10 min preheating cycle to soften the material. This was followed by several venting steps, and the material was pressed with a constant applied force of 16 MPa between both plates for 15 min. The square materials were then cured at 60 °C in an oven for 48 h and postcured for 24 h at room temperature.

Study of Self-Healing Behavior The macroscopic self-healing ability of material was analyzed on a dumbbell-shaped sample cut in half and then healed. The dumbbell was cut in the middle and subsequently healed by placing the halves in contact for 1 h at 120 °C, followed by 60 °C overnight, and then 24 h at room temperature and 50% RH, and was then tested by uniaxial tensile tests to evaluate the recovery of the integrity of the self-healed dumbbells.

Methods *Iodine Value* The iodine value (IV) was determined by using the Wijs method to quantify the double-bond content according to ISO 3961:2018(E).

Hydroxyl Value The hydroxyl value (HV) was determined by the esterification method using a 1 M solution of phthalic anhydride in pyridine (ASTM 4274-99) for the MO Diol and the biobased polyester polyol. The appropriate mass of sample was dissolved (1.25 g for MO Diol and 7.5 g for the polyester polyol) in 20 mL of phthalic anhydride solution, heated to 130 °C under reflux for 45 min, and cooled at room temperature. Pyridine was added (10 mL) from the top of the reflux to collect all reactions products; the last 20 mL of pyridine and 30 mL of water were added. The solution was titrated with 1 M potassium hydroxide (KOH) solution with phenolphthalein solution as indicator. The HV was determined in mg of KOH g^{-1}, as described in eq 2.

$$\mathrm{HV} = \frac{(V_{\mathrm{blank}} - V_{\mathrm{s}}) \times C \times 56.1}{W_{\mathrm{s}}} \quad (2)$$

where V_{blank} (mL) and V_{s} (mL) are the volumes of KOH solution required for blank and polyol sample titrations, respectively. C (mol L^{-1}) is the KOH solution concentration, and W_{s} (g) is the polyol weight.

NMR Spectroscopy All NMR spectra were recorded on a Bruker Ascend 400 or 500 MHz spectrometer. Sample were dissolved in deuterated chloroform ($CDCl_3$) or deuterated dimethyl sulfoxide ($[D_6]$DMSO) with contents between 8–10 and 20–30 mg/mL for ^{1}H NMR and ^{13}C NMR spectroscopy, respectively. The calibration of ^{1}H and ^{13}C NMR spectra was performed by using the chloroform peaks at δ = 7.26 and 77.16 ppm, respectively, and the DMSO peak at δ = 2.50 ppm as references. ^{31}P NMR analysis was performed by 2-chloro-4,4,5,5-tetramethyl-1,3,2-dioxaphospholane as a phosphylating agent. Scans (128) were recorded with a 15 s delay and a spectral width of 80 ppm (180–100 ppm). Cholesterol was used as an internal standard, as described in standard protocols.[36] In the case of quantitative ^{1}H NMR spectroscopic analysis, 20 mg was dissolved in $[D_6]$DMSO (0.5 mL) for each sample before the addition of a standard solution (100 μL) of pentafluorobenzaldehyde in $[D_6]$DMSO. Thirty-two scans were collected with 10 s delay.

Fourier Transform Infrared Spectroscopy (FTIR) For FTIR spectroscopy of experimental samples, a blank background was performed prior to examining samples (32 scans, resolution 4 cm^{-1}) on a Nicolet 380 spectrometer equipped with an ATR diamond module (FTIR-ATR) in reflection mode.

Thermal Gravimetric Analysis (TGA) Sample weighing between 1 and 3 mg were evaluated by TGA (TA Instruments Hi-Res TGA Q5000) at a heating rate of 10 °C min^{-1} from 25 to 700 °C, without oxidative atmosphere, under a nitrogen flow rate atmosphere at 25 mL min^{-1}.

Differential Scanning Calorimetry (DSC) In standard aluminum pans, samples between 1 and 3 mg in weight were examined by DSC (TA Instruments Q200) under a nitrogen flow at 50 mL min^{-1}. For cross-linked PUs, a single heating ramp of 10 °C min^{-1} was used over the same aforementioned temperature range. Non-cross-linked materials were evaluated by using a cyclical heating ramp.

Uniaxial Tensile Tests Uniaxial tensile testing was performed on an Instron model 5567 H, USA, at strain rate of 20 mm min^{-1} on dumbbell specimens of approximately 30 × 5 × 1 mm^3. For each synthesized or reprocessed PU, five dumbbell samples were tested.

Swelling Index and Gel Content Determination The swelling ratio (SR) for each PU was determined between dried (m_{i}) and swollen samples (m_{s}) in DMF according to eq 3.

$$\mathrm{SR} = \frac{m_{\mathrm{s}} - m_{\mathrm{i}}}{m_{\mathrm{i}}} \times 100 \quad (3)$$

PU samples of approximately 10–20 mg were swollen in 15 mL of solvent over an entire day. Three repetitions were examined for each PU formulation. The insoluble fraction (IF) was determined by drying the swollen sample (m_{f}) according to eq 4:

$$\mathrm{IF} = \frac{m_f}{m_i} \times 100 \qquad (4)$$

Small- and Wide-Angle X-ray Scattering (SWAXS) The SWAXS patterns were obtained with a transmission Guinier-like geometry. A linear focalized monochromatic Cu $K\alpha_1$ beam (λ = 1.5405 Å) was obtained by using a sealed-tube generator (600 W) equipped with a bent quartz monochromator. In all cases, samples were filled in homemade cells of 1 mm path. The scattering curves were recorded with a curved Inel CPS120 counter gas filled and corrected from air scattering contribution.

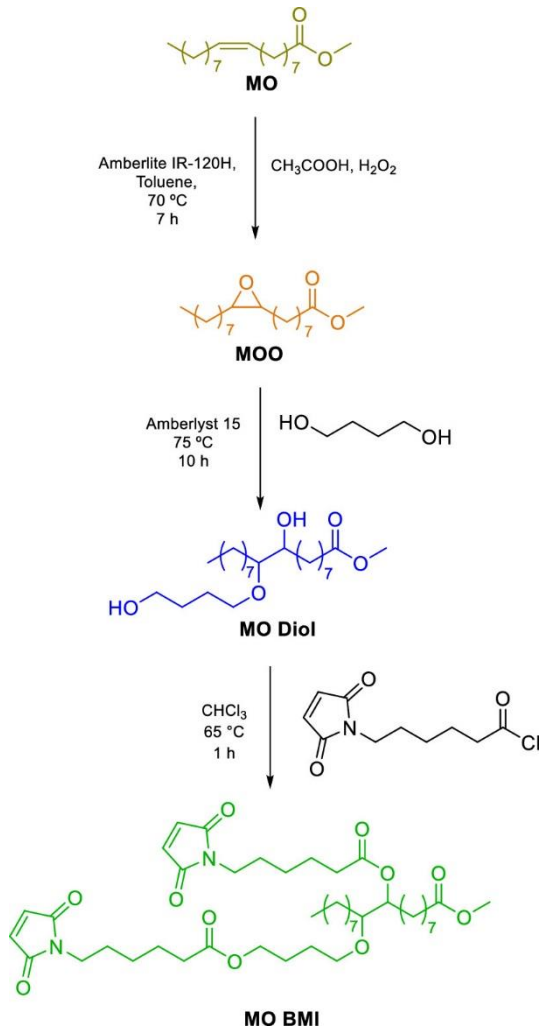

Scheme 2. Global Reaction Pathway of MO BMI

Results and Discussion

Analysis of Synthesis of MO BMI The alkene moiety of methyl oleate (MO) was used as the reaction site to yield a MO-based BMI as depicted in Scheme 2. First, MO underwent an *in situ* epoxidation with peroxyacetic acid as the oxidizing agent to yield MOO. This type of epoxidation is routinely used on vegetable oils.[37] Other pathways for epoxidations using, for example, presynthesized oxidizing agents such as *m*-chloroperoxybenzoic acid (mCPBA) require large quantities of solvents. Thus, the *in situ* epoxidation method abides more precisely to the principles of green chemistry. The FTIR spectrum

of MOO (Figure 1b) shows the disappearance of the double bonds at $\tilde{\nu}$ = 3009 cm^{-1} and the appearance of the C–H bending associated with appearance of epoxides at $\tilde{\nu}$ = 825 cm^{-1}. By ^{1}H NMR spectroscopic analysis (Figure 2b), the structure is confirmed with the disappearance of the vinyl and allyl protons at δ = 5.35 and 2.0 ppm, respectively, and by the appearance of the epoxide and protons alpha to the epoxides at δ = 2.90 and 1.45 ppm, respectively. The results of the ^{13}C NMR spectroscopic analysis of MOO agreed with the assigned structure as depicted in Figure S1 of the Supporting Information.

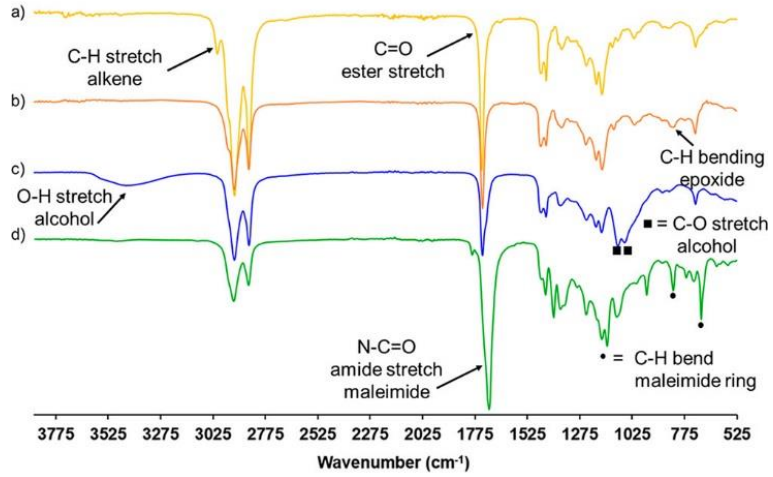

Figure 1. FTIR spectra (a) MO, (b) MOO, (c) MO Diol, and (d) MO BMI with the assignations of the main peaks.

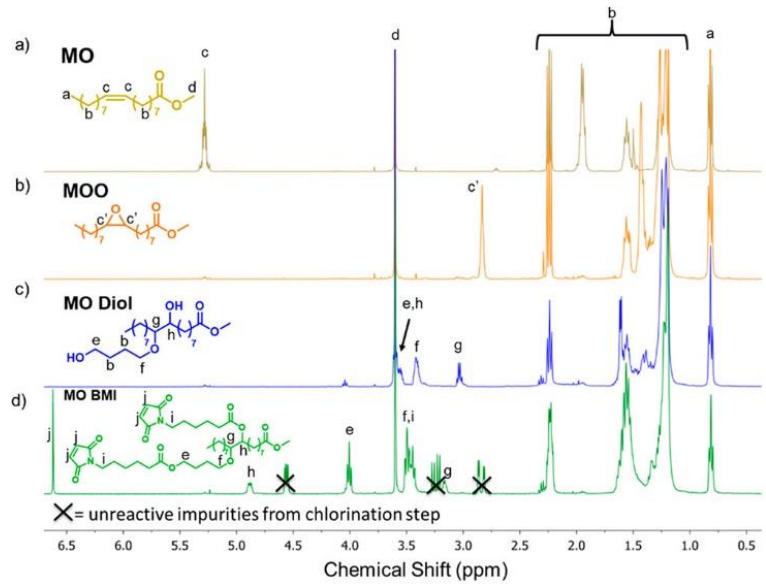

Figure 2. ^{1}H NMR spectra of (a) MO, (b) MOO, (c) MO Diol, and (d) MO BMI, with the assignations of the main signals and the corresponding chemical structures.

Thereafter, MOO underwent a ring-opening reaction with BDO to give MO Diol as the main product along with a diester diol as a side product (chemical structure in Figure S2). This diester as a side product is shown also by size exclusion chromatography (SEC) as depicted in Figure S3. The protocol developed by Palaskar et al. was slightly altered and improved.[38] The reaction was for instance limited

to 10 h compared to 20 h, since the transesterification between the ester moiety and BDO largely took place after 10 h. Figure S4 illustrates that at 10 h all epoxy moieties have been opened by BDO,and the transesterification reaction begins to take place. Furthermore, the purification step for the removal of BDO consisted solely of water-based washing as opposed to vacuum distillation to avoid further side reactions. The HV was determined by two methods: a chemical esterification titration method using phthalic anhydride and quantitative ^{31}P NMR which gave similar and reproducible results (Figure S5 and Table S1). The HV of MO Diol is 223 mg of KOH/g. This is relatively close to the theoretical value of 258 mg of KOH/g if only the MO Diol product was achieved without diester side product. The FTIR spectrum of MO Diol (Figure 1c) shows the disappearance of C–H bending associated with the epoxides at $\tilde{\nu}$ = 825 cm^{-1}, the appearance of a broad band between $\tilde{\nu}$ = 3600 and 3100 cm^{-1} corresponding to the hydroxyl groups, and the appearance of a C–O stretch of newly formed alcohols. The ^{1}H NMR spectrum of the MO Diol along with proton assignments is presented Figure 2c. The chemical structure of MO Diol is confirmed by the appearance of peaks at δ = 3.65 ppm (e) (CH_2OH), 3.60 ppm (h) (CH–OH), 3.47 ppm (f) (CH_2OCH), and 3.10 ppm (g) the proton adjacent to ether bond. The results of the analysis of ^{13}C NMR of the MO Diol agreed with the assigned chemical structure as depicted in Figure S1.

MO BMI was finally synthesized by the esterification of the hydroxyl groups of MO Diol by 6-MHA. Similarly to previously reported work,[26,27] 6-MHA was transformed into an acyl chloride derivative, 6-MHC, to increase the reactivity of the reaction (Scheme S1). The success of this transformation reaction is attested by the ^{1}H NMR spectra of 6-MHA and 6-MHC and the corresponding proton assignments found in Figure S6. The derivatization of MO Diol was then conducted by using 1.2 equiv of 6-MHC under catalyst-free conditions to Figure 2d), ^{13}C NMR (Figure S1), SEC, and quantitative ^{1}H NMR (Figure S7) to determine the maleimide content of MO BMI reported to be 1.83 mmol/g. The FTIR spectrum of MO BMI evidenced the disappearance of a broad band between $\tilde{\nu}$ = 3600 and 3100 cm^{-1} corresponding to the hydroxyl groups and C–O stretch of alcohols. Furthermore, the N–C═O amide stretch of the maleimide ring is detected at $\tilde{\nu}$ = 1701 cm^{-1} as well as the C–H bend associated with the maleimide ring at $\tilde{\nu}$ = 826 and 696 cm^{-1}. The ^{1}H NMR spectrum of MO BMI was analyzed and evidenced by the appearance of a strong signal at δ = 6.7 ppm belonging to the maleimide ring double-bond protons. The SEC chromatograms of MO BMI, MO Diol, and 6-MHA are presented in Figure S3. When evaluating these chromatograms purely in terms of retention times, we observed that MO BMI has an increased retention time in comparison to the MO Diol starting material due to the successful esterification by 6-MHC. Nevertheless it is important to note that within the chromatogram of MO BMI the evidence of the excess use of 6-MHC is clearly observed at lower retention times (∼8.7 min) where a weight-average molar mass corresponding to 6-MHA is seen. Quantitative ^{1}H NMR (in [D_6]DMSO) was used to determine the maleimide content by using the C–H bending signal at δ = 7.1 ppm as this signal is free from overlap from other MO Diol signals. This calculation is further depicted by Figure S7 and Table S2.

Analysis of DA Cycloaddition of MO BMI and FDM To confirm and study the DA adduct formation by ^{1}H NMR of MO BMI when exposed to furan moieties, MO BMI was reacted with FDM in DMSO at 65 °C (Figure 3a). As depicted in Figure 3b, the ^{1}H NMR spectrum and proton assignment confirm the formation of the DA adduct. The proton assignment was confirmed by using the ^{1}H NMR of initial reactional entities and compared to the literature.[39] To quantify the conversion, proton signals f_1 (in the furan) and f_1′ (in the adduct) were used as they are free from overlap with other signals (Figure 3b). The conversion was calculated by eq 5 for the proton set f_1 and f_1′ as follows:

$$X\ (\%) = \frac{\mathrm{Int}_{f_1'}}{\mathrm{Int}_{f_1} + \mathrm{Int}_{f_1'}} \times 100 \qquad (5)$$

where Int_{f1} and Int_{f1}' represent the integral values of their respective protons. In Figure 3c, the trend of the conversion with respect to time at 65 °C is shown. As similarly reported in the literature,[40,41] an equilibrium conversion of 88% was obtained after 78 h of reaction time. A limited conversion was reached due to the thermodynamic equilibrium between the forward and retro reaction at 65 °C.[27,40,41] Decreasing the reaction temperature could increase the final conversion, nevertheless leading to slower reaction kinetics. Moreover, proton signals f_1' were used to assess the presence of the two diastereomers of the DA adduct (endo and exo) with respect to time (Figure 3b), as the chemical shift differs for each diastereomer. The kinetically favored endo adduct is first formed at 80%. An equilibrium between the two diastereomers starts after 78 h (50 wt %).

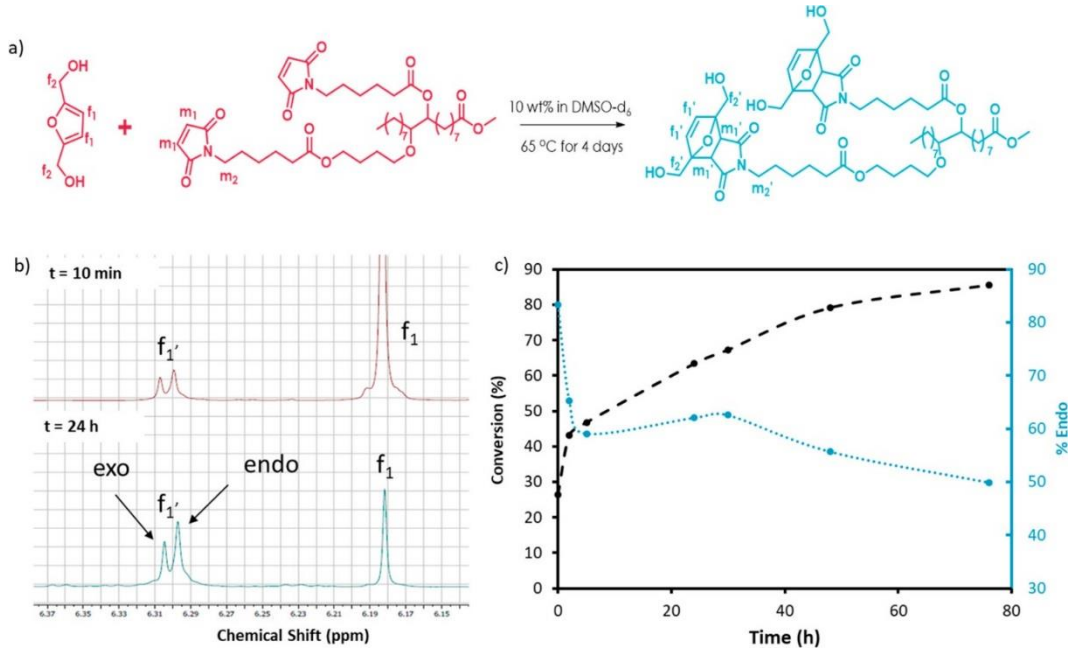

Figure 3. (a) Reaction scheme between FDM and MO BMI. (b) ^{1}H NMR of spectra of mixture of FDM and MO BMI after 10 min and 24 h. (c) Conversion and percentage of endo structure with respect to time and 65 °C.

Analysis of the Synthesis of Biobased Cross-Linked PUs Cross-linked biobased PUs containing thermoreversible DA adducts were synthesized. Scheme 1 depicts the synthesis of (i) the control systems (linear PUs; recations 1 and 2) and (ii) the cross-linked PUs (reactions 1-3). Furthermore, the synthesis of the PU control systems and PU backbone used for cross-linked PUs was represented structurally in Scheme S2. Different PUs were obtained by varying the HS% in the PU structure. The HS% is the mass of HDI and FDM with respect to the mass of the global structure. The HS% in the PU systems was varied either as 5, 10, or 20%. The nomenclature of all PU systems prepared is summarized in Table 1. As previously mentioned, three different BMIs were explored as cross-linkers: a synthesized biobased BMI, MO BMI, and two fossil-based BMIs. The fossil-based aromatic BMI chosen was MP BMI, and the aliphatic fossil-based BMI chosen was PPO BMI. The chemical structures of both these conventional fossil-based BMIs are illustrated in Figure 4.

Table 1. Linear PU (Control) and Cross-Linked Systems: Nomenclature and Corresponding Formulations

PU system	type of system	HS content [%]	type of BMI cross-linker
PU-HS5	linear	5	N/A
PU-HS10	linear	10	N/A
PU-HS20	linear	20	N/A
PU-HS5-MOBMI	cross-link	5	MO BMI
PU-HS10-MOBMI	cross-link	10	MO BMI
PU-HS20-MOBMI	cross-link	20	MO BMI
PU-HS20-MPBMI	cross-link	20	MP BMI
PU-HS20-PPOBMI	cross-link	20	PPO BMI (DP = 3)

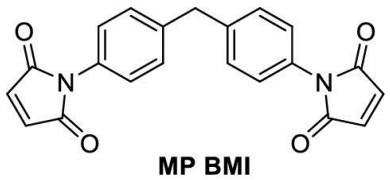

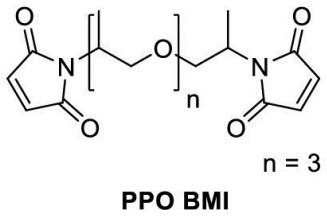

Figure 4. Chemical structure of both conventional maleimide-terminated BMIs used as cross-linkers.

All PU networks after postcuring (linear and cross-linked) were insoluble in conventional solvents ($CHCl_3$, DMSO, THF, and DMF) and were thus examined by FTIR. In Figure 5, a comparison of the FTIR spectra of PU-HS5, PU-HS10, PU-HS20, polyester polyol, and FDM is presented. In the spectra of the three linear control PUs (Figure 5a–c), no peak was found at $\tilde{\nu}$ = 2270 cm^{-1} (NCO stretching band), and the disappearance the hydroxyl stretches (approximately at $\tilde{\nu}$ = 3600 to 3025 cm^{-1}) associated with the hydroxyls of polyester polyol and FDM is observed. Furthermore, the FTIR spectra of PU-HS5, PU-HS10, and PU-HS20 could be used to highlight the main structural differences between them. As expected, the main variations are related to the increasing content of HS%, leading to higher concentration of urethane groups (−NH–C═O–O−). This is highlighted by the increasing vibrations of −NH stretching and bending ($\tilde{\nu}$ = 3335 and 1550 cm^{-1}, respectively) as well as the C═O stretching from the urethane group ($\tilde{\nu}$ = 1680 cm^{-1}) from PU-HS5 to PU-HS20.

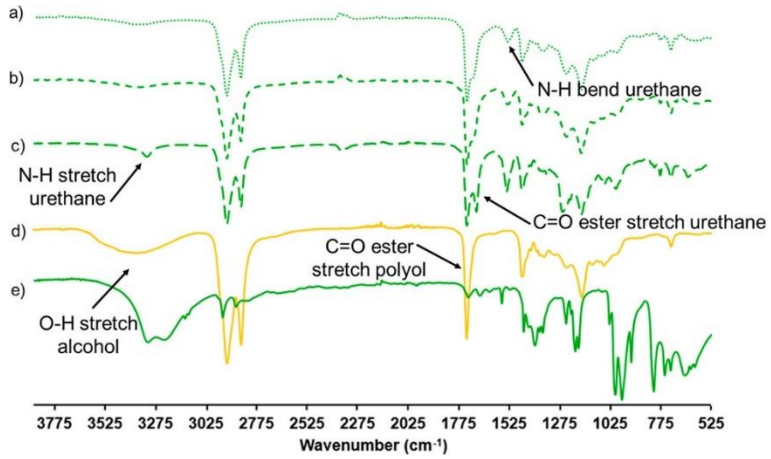

Figure 5. FTIR spectra of from top to bottom: (a) PU-HS5, (b) PU-HS10, (c) PU-HS20, (d) rapeseed-based polyol, and (e) FDM.

The FTIR spectra of all cross-linked PU networks compared to their control PU and bismaleimides are displayed in Figure 6 and Figure S8. Figure 6 displays the FTIR spectra of PU-HS20 (Figure 6a) compared to the cross-linked PU networks PU-HS20-PPOBMI (Figure 6b), PU-HS20-MPBMI (Figure 6d), and PU-HS20-MOBMI (Figure 6f) with their respective BMIs: PPO BMI (Figure 6c), MP BMI (Figure 6e), and MO BMI (Figure 6g). The FTIR spectrum of MP BMI distinguishes itself by the C–C stretches of the aromatic ring at $\tilde{\nu}$ = 1500 cm^{-1} (Figure 6e). It was observed that PS-HS20-PPOBMI and PU-HS20-MPBMI lose the prevalence of the peaks associated with the HS concentration (N–H stretch, bend, and urethane C═O ($\tilde{\nu}$ = 1550 cm^{-1}). In Figure S8 it can be observed that for each PU network cross-linked with MO BMI, PU-HS5-MOBMI (Figure S8b), PU-HS10-MOBMI (Figure S8d), and PU-HS20-MOBMI (Figure S8f), the carbonyl stretch corresponding to the urethane of the control PU-HS5 (Figure S8a), PU-HS10 (Figure S8c), and PU-HS20 (Figure S8e) becomes masked by the carbonyl stretch of the amide of the maleimide. Furthermore, the N–H stretch of the urethane at ($\tilde{\nu}$ = 3335 cm^{-1}) becomes slightly less prevalent, most specifically in the case PU-HS20-MOBMI. Moreover, as all PU cross-linked networks are cross-linked via DA reaction, the disappearance of the C–H bending of maleimide ring ($\tilde{\nu}$ = 826 and 692 cm^{-1}) is observed.

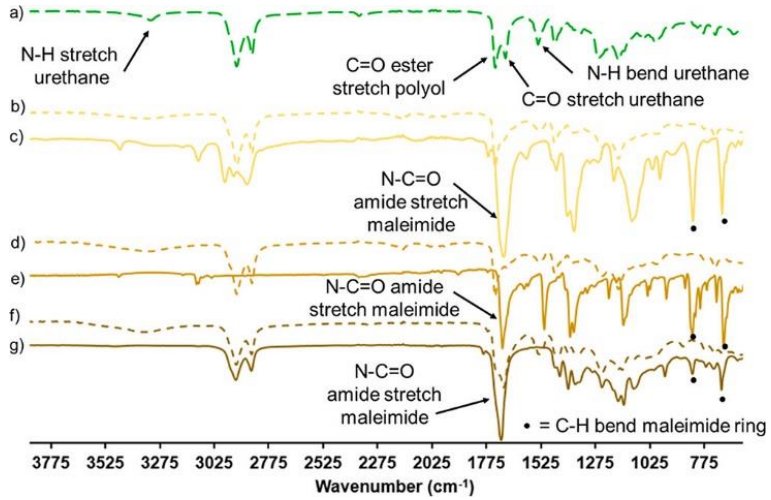

Figure 6. FTIR spectra of from top to bottom: (a) PU-HS20, (b) PU-HS20-PPOBMI, (c) PPO BMI, (d) PU-HS20-MPBMI, (e) MP BMI, (f) PU-HS20-MOBMI, and (g) MO BMI.

Mechanical, Thermal, and Structural Evaluations of Biobased Cross-Linked PUs TGA was used to evaluate the thermal stability of PU materials. Detailed TGA results can be found in Figure S9. In Table 2, the initial thermal degradation ($T_{5\%}$) is reported. The $T_{5\%}$ for all materials is considerably above the r-DA reaction of ∼120 °C, allowing for the r-DA reaction to take place without any significant thermal degradation of materials. Control PUs (PU-HS5, PU-HS10, and PU-HS20) exhibit decreased $T_{5\%}$ with increasing HS ratio. As described in a previous study of our group,[42] for equivalent biobased PU materials, initial degradation takes place in the HS domain, and the thermal degradation is directly linked to the HS content. When comparing control PUs with their respective cross-linked materials, the $T_{5\%}$ decreased for cross-linked materials. This is primarily linked to the thermal degradation of the BMIs used. As previously mentioned, the temperature at which the initial thermal degradation takes place for cross-linked materials is above that of the r-DA, thus allowing the degradation of free BMIs to take place. The range at which initial degradation begins in cross-linked PUs is well pass the temperature at which significant degradation takes place for the reported BMIs. This is adamant when comparing control PUs to their counterparts cross-linked by MO BMI. The prevalence of MO BMI considerably decreases the $T_{5\%}$ due to its decreased thermal stability. Furthermore, upon comparison of $T_{5\%}$ of control PU-HS20 to cross-linked PU materials, the lowest $T_{5\%}$ reported is that of PU-HS20-MOBMI, whereas PU-HS20-PPOBMI and PU-HS20-MPBMI were observed to be 30 °C higher due to their respective higher thermal stability. This can be linked to the long-chain aliphatic nature of MO BMI as well as traces of reagents from synthesis of MO BMI allowing for lower thermal stability. In contrast, the PU material PU-HS20-MPBMI exhibits the highest $T_{5\%}$ in comparison to other cross-linked PU-HS20 materials, and this could be related to the aromaticity of the cross-linker allowing for higher thermal stability.

The glass transition temperatures (T_g) were determined by DSC. To avoid degradation, the T_g of all materials were recorded from −80 to 175 °C as reported in Table 2. A single heating ramp was used for cross-linked PUs. Detailed DSC thermograms can be found in Figure S10. The T_g of all PU materials were observed in a very short window, from −51 to −48 °C. As a general trend, the T_g of cross-linked materials increased (due to cross-linking) when compared to their control counterparts with the exception of PU-HS5-MOBMI. Endothermic peaks corresponding to the r-DA reaction did not seem to appear clearly in any cross-linked PU due to the consequently predominant T_g related to the HS domains and could not be studied.

The mechanical properties of all PUs were evaluated at room temperature by uniaxial tensile tests. They are reported in Table 2 and Figure S11. For control PUs, results indicated that increased HS content led to increased tensile strength and decreased elongation, with the exception of PU-HS5, which exhibited a predictable lower tensile strength but also surprisingly lower elongation at break. As expected, the Young's modulus increased due to the increasing HS content of the control PU materials. For PU materials that are cross-linked by MO BMI (Figure S11a), the building block MO BMI tends to have a softening effect compared to the other systems. These PU materials present an increased elongation break and a strong decrease in Young's modulus and tensile strength. This behavior was most apparent in PU-HS10-MOBMI and PU-HS20-MOBMI. This can be explained by the aliphatic and branched long chains of MO BMI. Furthermore, as MO BMI was synthesized with an excess of 6-MHC, the neutralized 6-MHC by methanol gave the corresponding methyl ester, which certainly cause soften in the materials. Nevertheless, the cross-linking does not counter this softening effect due to MO BMI architecture or of remnant reagents. In contrast, PU-HS20 cross-linked by conventional BMIs PPO BMI and MP BMI led to the expected increase in Young's modulus and tensile strength but surprisingly similar elevated elongation at break (Figure S11b). Other research groups have used FDM as part of synthesis of polymer backbones, such as polyesters[43] and PUs,[44] both cross-linked by varying amounts of MP BMI, where the PU study exhibited similar behavior. This could perhaps be explained

by the fact that the cross-linking took place in the HS domain. This could be further developed in studying PU networks with constant HS content and cross-linked by varying the amount of BMI. Given that the cross-linking takes places in the HS, there seems to be an interplay between the phase segregation of the materials and the DA reaction, especially evident with short BMIs. This was further investigated by small- and wide-angle X-ray scattering (SWAXS) to observe the SWAXS patterns of these PUs. Nevertheless, it is apparent the structure of the BMIs played an evident role in improving the material properties, as PU-HS20-MPBMI reported higher Young's modulus than PU-HS20-PPOBMI. However, the PUs cross-linked with different conventional BMIs reported similar tensile strength.

Table 2. Main Characterizations of Synthesized Biobased PUs

PU system	TGA $T_{5\%}$ [°C]	DSC T_g [°C]	Young's modulus MPa]	σ[a] [MPa]	ε[b] [%]	SR[c] in DMF [%]	IF[d] [%]
PU-HS5	348	–49	2.33 ± 0.21	0.55 ± 0.01	91 ± 14	40 ± 3	97.6 ± 0.1
PU-HS10	322	–49	2.73 ± 0.15	0.88 ± 0.01	155 ± 4	167 ± 18	97.5 ± 4.4
PU-HS20	281	–51	5.64 ± 1.12	1.73 ± 0.08	74 ± 8	137 ± 6	93.5 ± 1.0
PU-HS5-MOBMI	339	–51	1.80 ± 0.12	0.57 ± 0.02	102 ± 13	42 ± 1	96.4 ± 0.1
PU-HS10-MOBMI	298	–48	3.80 ± 0.05	0.35 ± 0.01	299 ± 15	105 ± 2	91.2 ± 1.6
PU-HS20-MOBMI	230	–51	0.17 ± 0.01	0.15 ± 0.01	114 ± 9	116 ± 5	84.8 ± 3.0
PU-HS20-PPOBMI	261	–48	6.20 ± 1.03	2.28 ± 0.21	114 ± 9	70 ± 11	97.1 ± 1.3
PU-HS20-MPBMI	268	–48	13.4 ± 1.81	2.07 ± 0.06	97 ± 12	69 ± 2	96.1 ± 0.6

[a]Tensile strength. [b]Elongation. [c]SR = swelling ratio. [d]IF = insoluble fraction.

All PUs were characterized by swelling tests in DMF. Results are reported in Table 2. The PUs cross-linked by MO BMI appear to have decreased swelling ratios (SRs) with respect to the linear counterpart but as well experienced decreased in insolubility fraction (IF). This is highly likely due to remnants reagents and byproducts carried over from the MO BMI synthesis, as depicted in the ^{1}H NMR and ^{13}C NMR spectroscopic analyses (Figure 2 and Figure S1). Some questions remain open, and at this level it is difficult to fully conclude whether the decreasing in swelling is solely due to cross-linking or rather soluble mass transferred to the organic solvent phase. Additional investigations could be needed on this point. In contrast, a significant decrease in SRs and increase in IFs is evidently apparent in PUs cross-linked by the conventional BMIs.

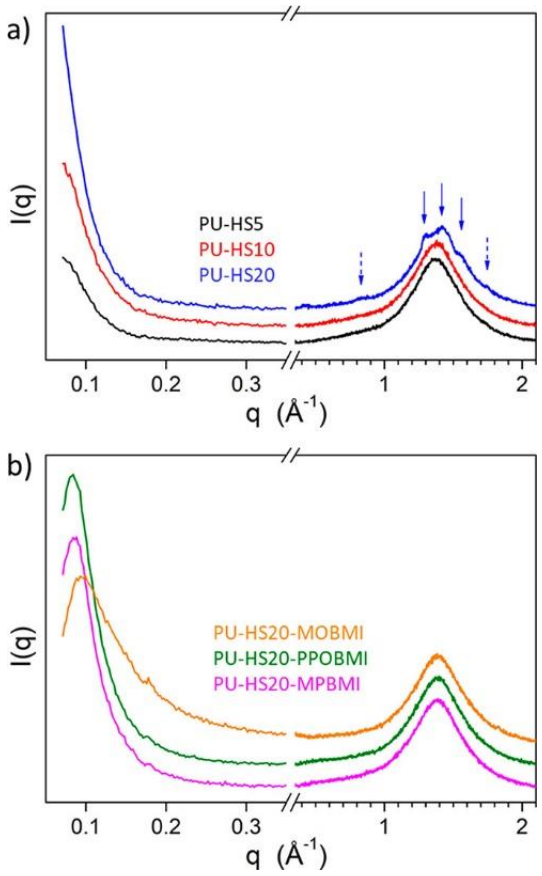

Figure 7. SWAXS patterns of (a) PU-HS5, PU-HS10, and PU-HS20 and (b) PU-HS20-MOBMI, PU-HS20-PPOBMI, and PU-HS20-MPBMI.

Lastly, the SWAXS patterns of some synthesized PUs are shown in Figure 7. As shown in Figure 7a, from the PU-HS5 and PU-HS10 curves, it cannot be excluded that the appearance of an upturn instead of a peak pertains to a completely irregular distribution of hard and soft segments. However, the explanation is more probably the same as for PU-HS20, with namely the presence of a crystalline fraction. The steep upturn shown by PU-HS20 and above all the broadened reflections overlapping the broad wide-angle signal (blue arrows) are indeed clear proof for a scattering contribution from crystallites dispersed in the amorphous matrix. This contribution masks the peak from hard–soft alternation in PU-HS20 and probably also in PU-HS10 and PU-HS5. The average crystallite size in PU-HS20 is ∼10 nm, as estimated from reflection width using the Scherrer equation with shape factor K = 0.9. As depicted in Figure 7b, in addition to the wide-angle scattering signal at 1.4 $Å^{-1}$ from lateral distances between molecular segments, patterns exhibit a broad peak in the small-angle range reflecting the hard–soft alternation in the elastomeric structure.[45] The periodicity of this alternation, i.e., the long period $L = 2p/q^*$ deduced from peak maximum q^*, is 74–75 Å for PU-HS20-MOBMI, 75–76 Å for PU-HS20-PPOBMI, and 65–66 Å for PU-HS20-MPBMI. The thickness of the hard segments slabs, i.e., the short period S deduced from the scattering profile using the one-dimensional correlation function,[46] is 15 Å for PU-HS20-MOBMI and PU-HS20-PPOBMI and 12 Å for PU-HS20-MPBMI. However, the hard segment slabs are constituted of neat HDI or of HDI juxtaposed to furan and possibly engaged in adduct with bismaleimide. These elastomers are indeed more complex than the two-phase model used for the scattering curve analysis, and the short periods therefore represent average values of the weighted individual hard segment configurations.

Evaluation of the Remendable and Self-Healing Behaviors As an advanced property, reprocessability was studied by using PU materials cross-linked by conventional BMIs and PU-HS10-MOBMI and

reported in Figure 8 and Table S3. The reprocessability of these PUs was evaluated by comparing the mechanical properties of original materials processed by solvent casting to materials reprocessed by compression molding. Of all materials evaluated, PU-HS10-MOBMI seems to best preserve its static mechanical properties over two hot press reprocessing cycles, with only experiencing a loss in Young's modulus after a second reprocessing cycle. PU-HS20-PPOBMI seems to preserve its Young's modulus over all processing cycles whereas PU-HS20-MPBMI evidenced an apparent decrease over reprocessing cycles. Although the aromatic nature for the MP BMI yields superior mechanical properties, it can affect the reprocessing ability of the material by compression molding. The high melting temperature of MP BMI (∼150 °C) can be affecting the reprocessing ability of materials, specifically during the curing step (DA reaction) of the procedure as this limits the local mobility of MP BMI in the material. Nevertheless, PU-HS20-MPBMI loss in Young's modulus and tensile strength remains quantitatively superior than PU-HS20-PPOBMI for the respective reprocessing step. The notable lack of preservation of material properties over processing cycles can be attributed to the inability of the material to maintain its cross-linking density when exposed to this thermal treatment. As previously mentioned, dissociative CANs often exhibit varying cross-link densities after reprocessing, which in turn affect the mechanical properties due to chain rearrangement, vitrification, and cross-link ruin.[19] Furthermore, since there is an interplay between the hydrogen bonding due to the phase segregation of the materials and the DA reaction, exposing the material to different reprocessing procedures could enhance reprocessability. For example, curing temperatures higher than 60 °C but lower than 90 °C, for the DA reaction to take place, could increase the kinetics of the DA reaction in the material but as well enhance local mobility.

As an advanced property, the self-healing ability of PU-HS10-MOBMI was also evaluated. The initial 120 °C heating allows the r-DA to take place but as well as promotes adhesion, whereas the 60 °C heating cycle allows for the network to be re-formed by the DA reaction. After thermal treatment, the cut dumbbells have recovered their integrities. As depicted in the stress–strain curved of the initial and healed sampled displayed in Figure 9, the healed sample seems to almost fully recover in Young's modulus and attain about 50% of the initial tensile strength. Because of their toughness, PU-HS20-PPOBMI and PU-HS20-MPBMI samples could not be easily tested for self-healing. In contrast, an adhesion test could be further developed to further characterize these stiffer materials by examining the adhesion between two pieces of these material on larger surfaces areas.

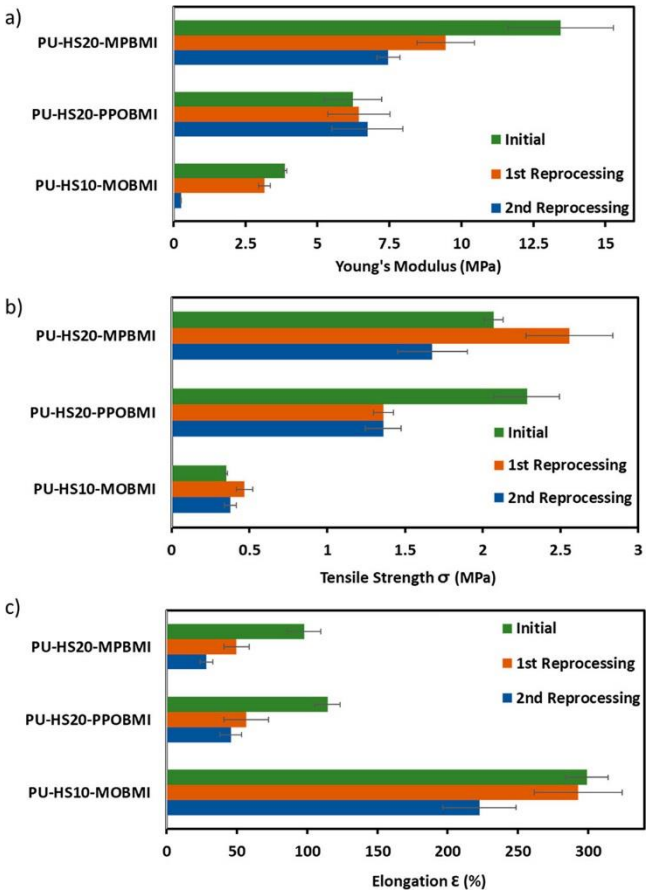

Figure 8. Uniaxial tensile tests to compare the mechanical results of initial and reprocessed materials PU-HS20-MPBMI, PU-HS20-PPOBMI, and PU-HS10-MOBMI: (a) Young's modulus, (b) tensile strength (σ), and (c) elongation (ε).

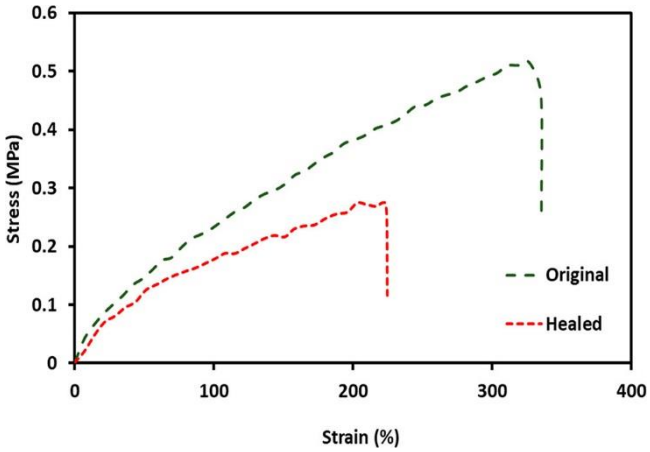

Figure 9. Uniaxial tensile tests: stress–strain curves of healed samples PU-HS10-MOBMI.

Conclusion

A new approach of producing cross-linked vegetable oil-based PUs via the thermoreversible furan–maleimide DA reaction was studied and successfully developed. Linear PUs were synthesized by using

rapeseed-based polyol, HDI, and FDM, a furan containing chain extender. By using FDM as chain extender, we can explore the cross-linking of PUs in the HS domain. The furan content was varied in PUs by varying the HS content (5, 10, and 20%). Furthermore, to ultimately avoid the use of fossil-based BMIs and provide a new branched BMI, an original biobased methyl oleate BMI (MO BMI) derived from sunflower oil was synthesized and fully characterized. The PUs were cross-linked by MO BMI as well as two conventional and fossil-based BMIs: 1,1′-(methylenedi-4,1-phenylene)bismaleimide and PPO-based BMI. Control PUs (without BMI cross-linking) generally exhibited increased Young's modulus and tensile strength and decreased elongation with increasing HS content. However, when these PUs were cross-linked by MO BMI, MO BMI tends to have a softening effect on the material, with increased elasticity. The long branched aliphatic chains of MO BMI as well of shortcomings of its synthesis process can be attributed to the reported behavior. In contrast, PUs cross-linked with shorter linear BMIs would yield increased Young's modulus, tensile strength, T_g, and IF and decreased SR. PUs cross-linked by MO BMI exhibited the most consistent thermal recyclability and heat-induced self-healing. Nevertheless, PUs cross-linked by conventional BMIs showed promising thermal recyclability which requires further optimization by modified thermal treatments. Future efforts consist of further examining the temperature-dependent viscoelastic behavior of these CANs to further improve thermal recyclable behavior.

These PU networks are reported for the first time with such a high biobased content (90 wt %). Synthesizing such networks provides a holistic approach to sustainable material design by incorporating sustainable raw materials but as well as attempting to control the end life of materials as a means to reduce energy and waste. This innovative work contributes to the development of biobased intrinsically dynamic architectures for a wide range of material domains.

SUPPORTING INFORMATION

The Supporting Information is available free of charge at
https://pubs.acs.org/doi/10.1021/acs.macromol.0c01115.

FUNDING

This study was funded by the Programme d'investissements d'avenir (PIA) of BPI-France.

NOTES

The authors declare no competing financial interest.

ACKNOWLEDGMENTS

The authors thank Programme d'investissements d'avenir (PIA) of BPI-France for their financial support and Iterg (France) for kindly providing technical grade methyl oleate. The authors also thank the R&D Team of Soprema (France). In memory of Pr. Jean-Pierre Pascault (1943–2020), a top researcher and great man who has always sympathetically followed the project.

ABBREVIATIONS

6-MHA, 6-maleimidohexanoic acid; 6-MHC, 6-maleimidohexanoyl chloride BDO, 1,4-butanediol; BMI, bismaleimide; CAN, covalent adaptable network; DA, Diels–Alder; DSC, differential scanning calorimetry; FDM, (furan-2,5-diyl)-dimethanol; HDI, hexamethylene diisocyanate; HS, hard segments; HV, hydroxyl value; IF, insolubility fraction; IV, iodine value; MO, methyl oleate; MO Diol, methyl 10-hydroxy-9-(4-hydroxybutoxy)octadecanoate; MOO, methyl 8-(3-octyloxiran-2-yl)octanoate; MP BMI, 1′ -(methylene-di-4,1-phenylene) BMI; Mw, weight-average molecular weight; NCO, isocyanate; PPO BMI, poly(propylene oxide)-based BMI; PU, polyurethane; r-DA, retro-Diels–Alder; SEC, size exclusion chromatography; SR, swelling ratio; SWAXS, small- and wide-angle X-ray scattering; TGA, thermal gravimetric analysis.

References

1. Staudinger, H. Über Polymerisation. *Ber. Dtsch. Chem. Ges. B* **1920**, *53* (6), 1073– 1085, DOI: 10.1002/cber.19200530627 [Crossref], [CAS], Google Scholar
2. Frey, H.; Johann, T. Celebrating 100 years of "polymer science": Hermann Staudinger's 1920 manifesto. *Polym. Chem.* **2020**, *11* (1), 8– 14, DOI: 10.1039/C9PY90161B [Crossref], [CAS], Google Scholar
3. Bioplastics, E. Bioplastics Market Development Update 2019. https://www.european-bioplastics.org/wp-content/uploads/2019/11/Report_Bioplastics-Market-Data_2019_short_version.pdf (accessed 16/12/2019).Google Scholar
4. Ronda, J. C.; Lligadas, G.; Galià, M.; Cádiz, V. Vegetable oils as platform chemicals for polymer synthesis. *Eur. J. Lipid Sci. Technol.* **2011**, *113* (1), 46– 58, DOI: 10.1002/ejlt.201000103 [Crossref], [CAS], Google Scholar
5. Lligadas, G.; Ronda, J. C.; Galia, M.; Cadiz, V. Renewable polymeric materials from vegetable oils: a perspective. *Mater. Today* **2013**, *16* (9), 337– 343, DOI: 10.1016/j.mattod.2013.08.016 [Crossref], [CAS], Google Scholar
6. Pan, X.; Sengupta, P.; Webster, D. C. High Biobased Content Epoxy–Anhydride Thermosets from Epoxidized Sucrose Esters of Fatty Acids. *Biomacromolecules* **2011**, *12* (6), 2416– 2428, DOI: 10.1021/bm200549c [ACS Full Text], [CAS], Google Scholar
7. Duarte, M. E.; Huber, B.; Theato, P.; Mutlu, H. The unrevealed potential of elemental sulfur for the synthesis of high sulfur content bio-based aliphatic polyesters. *Polym. Chem.* **2020**, *11* (2), 241– 248, DOI: 10.1039/C9PY01152H [Crossref], [CAS], Google Scholar
8. Hablot, E.; Donnio, B.; Bouquey, M.; Avérous, L. Dimer acid-based thermoplastic bio-polyamides: Reaction kinetics, properties and structure. *Polymer* **2010**, *51* (25), 5895– 5902, DOI: 10.1016/j.polymer.2010.10.026 [Crossref], [CAS], Google Scholar
9. Türünç, O.; Firdaus, M.; Klein, G.; Meier, M. A. R. Fatty acid derived renewable polyamides via thiol–ene additions. *Green Chem.* **2012**, *14* (9), 2577– 2583, DOI: 10.1039/c2gc35982k [Crossref], [CAS], Google Scholar
10. Tan, S. G.; Chow, W. S. Biobased Epoxidized Vegetable Oils and Its Greener Epoxy Blends: A Review. *Polym.-Plast. Technol. Eng.* **2010**, *49* (15), 1581– 1590, DOI: 10.1080/03602559.2010.512338 [Crossref], [CAS], Google Scholar
11. Hablot, E.; Zheng, D.; Bouquey, M.; Avérous, L. Polyurethanes Based on Castor Oil: Kinetics, Chemical, Mechanical and Thermal Properties. *Macromol. Mater. Eng.* **2008**, *293* (11), 922– 929, DOI: 10.1002/mame.200800185 [Crossref], [CAS], Google Scholar

12. Bueno-Ferrer, C.; Hablot, E.; Perrin-Sarazin, F.; Garrigós, M. C.; Jiménez, A.; Averous, L. Structure and Morphology of New Bio-Based Thermoplastic Polyurethanes Obtained From Dimeric Fatty Acids. *Macromol. Mater. Eng.* **2012**, *297* (8), 777– 784, DOI: 10.1002/mame.201100278 [Crossref], [CAS], Google Scholar
13. Desroches, M.; Escouvois, M.; Auvergne, R.; Caillol, S.; Boutevin, B. From Vegetable Oils to Polyurethanes: Synthetic Routes to Polyols and Main Industrial Products. *Polym. Rev.* **2012**, *52* (1), 38– 79, DOI: 10.1080/15583724.2011.640443 [Crossref], [CAS], Google Scholar
14. Pfister, D. P.; Xia, Y.; Larock, R. C. Recent Advances in Vegetable Oil-Based Polyurethanes. *ChemSusChem* **2011**, *4* (6), 703– 717, DOI: 10.1002/cssc.201000378 [Crossref], [PubMed], [CAS], Google Scholar
15. Carré, C.; Ecochard, Y.; Caillol, S.; Averous, L. From the synthesis of biobased cyclic carbonate to polyhydroxyurethanes: a promising route towards renewable non-isocyanate polyurethanes. *ChemSusChem* **2019**, *12*, 3410, DOI: 10.1002/cssc.201900737 [Crossref], [PubMed], [CAS], Google Scholar
16. Haponiuk, J. T.; Formela, K. In *Polyurethane Polymers*; Thomas, S., Datta, J., Haponiuk, J. T., Reghunadhan, A., Eds.; Elsevier: Amsterdam, 2017; Chapter 1, pp 1– 20.[Crossref], Google Scholar
17. Miao, S.; Wang, P.; Su, Z.; Zhang, S. Vegetable-oil-based polymers as future polymeric biomaterials. *Acta Biomater.* **2014**, *10* (4), 1692– 1704, DOI: 10.1016/j.actbio.2013.08.040 [Crossref], [PubMed], [CAS], Google Scholar
18. Fortman, D. J.; Brutman, J. P.; De Hoe, G. X.; Snyder, R. L.; Dichtel, W. R.; Hillmyer, M. A. Approaches to Sustainable and Continually Recyclable Cross-Linked Polymers. *ACS Sustainable Chem. Eng.* **2018**, *6* (9), 11145– 11159, DOI: 10.1021/acssuschemeng.8b02355 [ACS Full Text], [CAS], Google Scholar
19. Kloxin, C. J.; Scott, T. F.; Adzima, B. J.; Bowman, C. N. Covalent Adaptable Networks (CANs): A Unique Paradigm in Cross-Linked Polymers. *Macromolecules* **2010**, *43* (6), 2643– 2653, DOI: 10.1021/ma902596s [ACS Full Text], [CAS], Google Scholar
20. Denissen, W.; Winne, J. M.; Du Prez, F. E. Vitrimers: permanent organic networks with glass-like fluidity. *Chemical Science* **2016**, *7* (1), 30– 38, DOI: 10.1039/C5SC02223A [Crossref], [PubMed], [CAS], Google Scholar
21. Gandini, A.; Carvalho, A. J. F.; Trovatti, E.; Kramer, R. K.; Lacerda, T. M. Macromolecular materials based on the application of the Diels–Alder reaction to natural polymers and plant oils. *Eur. J. Lipid Sci. Technol.* **2018**, *120* (1), 1700091, DOI: 10.1002/ejlt.201700091 [Crossref], Google Scholar
22. Bergman, S. D.; Wudl, F. Mendable polymers. *J. Mater. Chem.* **2008**, *18* (1), 41– 62, DOI: 10.1039/B713953P [Crossref], [CAS], Google Scholar
23. Sun, H.; Kabb, C. P.; Sims, M. B.; Sumerlin, B. S. Architecture-transformable polymers: Reshaping the future of stimuli-responsive polymers. *Prog. Polym. Sci.* **2019**, *89*, 61– 75, DOI: 10.1016/j.progpolymsci.2018.09.006 [Crossref], [CAS], Google Scholar
24. Chen, X.; Dam, M. A.; Ono, K.; Mal, A.; Shen, H.; Nutt, S. R.; Sheran, K.; Wudl, F. A Thermally Re-mendable Cross-Linked Polymeric Material. *Science* **2002**, *295* (5560), 1698– 1702, DOI: 10.1126/science.1065879 [Crossref], [PubMed], [CAS], Google Scholar
25. Dhers, S.; Vantomme, G.; Avérous, L. A fully bio-based polyimine vitrimer derived from fructose. *Green Chem.* **2019**, *21* (7), 1596– 1601, DOI: 10.1039/C9GC00540D [Crossref], [CAS], Google Scholar
26. Duval, A.; Lange, H.; Lawoko, M.; Crestini, C. Reversible crosslinking of lignin via the furan-maleimide Diels-Alder reaction. *Green Chem.* **2015**, *17* (11), 4991– 5000, DOI: 10.1039/C5GC01319D [Crossref], [CAS], Google Scholar
27. Buono, P.; Duval, A.; Averous, L.; Habibi, Y. Thermally healable and remendable lignin-based materials through Diels – Alder click polymerization. *Polymer* **2017**, *133*, 78– 88, DOI: 10.1016/j.polymer.2017.11.022 [Crossref], [CAS], Google Scholar
28. Duval, A.; Couture, G.; Caillol, S.; Averous, L. Biobased and Aromatic Reversible Thermoset Networks from Condensed Tannins via the Diels-Alder Reaction. *ACS Sustainable Chem.*

Eng. **2017**, *5* (1), 1199– 1207, DOI: 10.1021/acssuschemeng.6b02596 [ACS Full Text], [CAS], Google Scholar
29. García-Astrain, C.; Avérous, L. Synthesis and evaluation of functional alginate hydrogels based on click chemistry for drug delivery applications. *Carbohydr. Polym.* **2018**, *190*, 271– 280, DOI: 10.1016/j.carbpol.2018.02.086 [Crossref], [PubMed], [CAS], Google Scholar
30. Yoshie, N.; Yoshida, S.; Matsuoka, K. Self-healing of biobased furan polymers: Recovery of high mechanical strength by mild heating. *Polym. Degrad. Stab.* **2019**, *161*, 13– 18, DOI: 10.1016/j.polymdegradstab.2019.01.007 [Crossref], [CAS], Google Scholar
31. Tremblay-Parrado, K. K.; Avérous, L. Renewable Responsive Systems Based on Original Click and Polyurethane Cross-Linked Architectures with Advanced Properties. *ChemSusChem* **2020**, *13*, 238, DOI: 10.1002/cssc.201901991 [Crossref], [PubMed], [CAS], Google Scholar
32. Hu, S.; Chen, X.; Torkelson, J. M. Biobased Reprocessable Polyhydroxyurethane Networks: Full Recovery of Crosslink Density with Three Concurrent Dynamic Chemistries. *ACS Sustainable Chem. Eng.* **2019**, *7* (11), 10025– 10034, DOI: 10.1021/acssuschemeng.9b01239 [ACS Full Text], [CAS], Google Scholar
33. Zhang, L.; Michel, F. C., Jr.; Co, A. C. Nonisocyanate route to 2,5-bis(hydroxymethyl)furan-based polyurethanes crosslinked by reversible diels–alder reactions. *J. Polym. Sci., Part A: Polym. Chem.* **2019**, *57* (14), 1495– 1499, DOI: 10.1002/pola.29418 [Crossref], [CAS], Google Scholar
34. Dolci, E.; Froidevaux, V.; Joly-Duhamel, C.; Auvergne, R.; Boutevin, B.; Caillol, S. Maleimides As a Building Block for the Synthesis of High Performance Polymers. *Polym. Rev.* **2016**, *56* (3), 512– 556, DOI: 10.1080/15583724.2015.1116094 [Crossref], [CAS], Google Scholar
35. Arbenz, A.; Perrin, R.; Avérous, L. Elaboration and Properties of Innovative Biobased PUIR Foams from Microalgae. *J. Polym. Environ.* **2018**, *26*, 254– 262, DOI: 10.1007/s10924-017-0948-y [Crossref], [CAS], Google Scholar
36. Spyros, A. Quantitative determination of the distribution of free hydroxylic and carboxylic groups in unsaturated polyester and alkyd resins by 31P-NMR spectroscopy. *J. Appl. Polym. Sci.* **2002**, *83* (8), 1635– 1642, DOI: 10.1002/app.10069 [Crossref], [CAS], Google Scholar
37. Petrović, Z. S.; Zlatanić, A.; Lava, C. C.; Sinadinović-Fišer, S. Epoxidation of soybean oil in toluene with peroxoacetic and peroxoformic acids—kinetics and side reactions. *Eur. J. Lipid Sci. Technol.* **2002**, *104* (5), 293– 299, DOI: 10.1002/1438-9312(200205)104:5<293::AID-EJLT293>3.0.CO;2-W [Crossref], [CAS], Google Scholar
38. Palaskar, D. V.; Boyer, A.; Cloutet, E.; Le Meins, J.-F.; Gadenne, B.; Alfos, C.; Farcet, C.; Cramail, H. Original diols from sunflower and ricin oils: Synthesis, characterization, and use as polyurethane building blocks. *J. Polym. Sci., Part A: Polym. Chem.* **2012**, *50* (9), 1766– 1782, DOI: 10.1002/pola.25944 [Crossref], [CAS], Google Scholar
39. Froidevaux, V.; Borne, M.; Laborbe, E.; Auvergne, R.; Gandini, A.; Boutevin, B. Study of the Diels–Alder and retro-Diels–Alder reaction between furan derivatives and maleimide for the creation of new materials. *RSC Adv.* **2015**, *5* (47), 37742– 37754, DOI: 10.1039/C5RA01185J [Crossref], [CAS], Google Scholar
40. Adzima, B. J.; Aguirre, H. A.; Kloxin, C. J.; Scott, T. F.; Bowman, C. N. Rheological and Chemical Analysis of Reverse Gelation in a Covalently Cross-Linked Diels-Alder Polymer Network. *Macromolecules* **2008**, *41* (23), 9112– 9117, DOI: 10.1021/ma801863d [ACS Full Text], [CAS], Google Scholar
41. Scheltjens, G.; Diaz, M. M.; Brancart, J.; Van Assche, G.; Van Mele, B. A self-healing polymer network based on reversible covalent bonding. *React. Funct. Polym.* **2013**, *73*, 413– 420, DOI: 10.1016/j.reactfunctpolym.2012.06.017 [Crossref], [CAS], Google Scholar
42. Bueno-Ferrer, C.; Hablot, E.; Garrigós, M. d. C.; Bocchini, S.; Averous, L.; Jiménez, A. Relationship between morphology, properties and degradation parameters of novative biobased thermoplastic polyurethanes obtained from dimer fatty acids. *Polym. Degrad.*

Stab. **2012**, *97* (10), 1964– 1969, DOI: 10.1016/j.polymdegradstab.2012.03.002 [Crossref], [CAS], Google Scholar
43. Zhang, Y.; Dai, Z.; Han, J.; Li, T.; Xu, J.; Guo, B. Interplay between crystallization and the Diels–Alder reaction in biobased multiblock copolyesters possessing dynamic covalent bonds. *Polym. Chem.* **2017**, *8* (29), 4280– 4289, DOI: 10.1039/C7PY00677B [Crossref], [CAS], Google Scholar
44. Gu, L.; Wu, Q. Y. Recyclable bio-based crosslinked polyurethanes with self-healing ability. *J. Appl. Polym. Sci.* **2018**, *135* (21), 46272, DOI: 10.1002/app.46272 [Crossref], Google Scholar
45. Charlon, M.; Heinrich, B.; Matter, Y.; Couzigné, E.; Donnio, B.; Avérous, L. Synthesis, structure and properties of fully biobased thermoplastic polyurethanes, obtained from a diisocyanate based on modified dimer fatty acids, and different renewable diols. *Eur. Polym. J.* **2014**, *61*, 197– 205, DOI: 10.1016/j.eurpolymj.2014.10.012 [Crossref], [CAS], Google Scholar
46. Goderis, B.; Reynaers, H.; Koch, M. H. J.; Mathot, V. B. F. Use of SAXS and linear correlation functions for the determination of the crystallinity and morphology of semi-crystalline polymers. *J. Polym. Sci., Part B: Polym. Phys.* **1999**, *37* (14), 1715– 1738, DOI: 10.1002/(SICI)1099-0488(19990715)37:14<1715::AID-POLB15>3.0.CO;2-F [Crossref], [CAS], Google Scholar